Transmissivity and groundwater flow exert a strong influence on drainage density

Elco Luijendijk[1]

[1]Independent scientist, Hanssenstrasse 7, 37073, Göttingen, Germany

Correspondence: Elco Luijendijk (elco.luijendijk@posteo.net)

Abstract. The extent to which groundwater flow affects drainage density and erosion has long been debated, but is still uncertain. Here, I present a new hybrid analytical and numerical model that simulates groundwater flow, overland flow, hillslope erosion and stream incision. The model is used to explore the relation between groundwater flow and the incision and persistence of streams for a set of parameters that represent average humid climate conditions. The results show that transmissivity

5 and groundwater flow exert a strong control on drainage density. High transmissivity results in low drainage density and high incision rates and vice versa, with drainage density varying roughly linearly with transmissivity. The model evolves by a process that is defined here as groundwater capture, whereby streams with a higher rate of incision draw the watertable below neighbouring streams, which subsequently run dry and stop incising. This process is less efficient in models with low transmissivity due to the association of low transmissivity and high watertable gradients. A comparison of different parameters

10 shows that drainage density is the most sensitive to transmissivity, followed by parameters that govern initial slope and stream erosion. These results imply that permeability and transmissivity exert a strong control on drainage density, stream incision and landscape evolution and that models of landscape evolution may need to explicitly include groundwater flow.

1 Introduction

15 Drainage density is a fundamental property of the earth's surface that controls erosion and the transport of water and sediments. Drainage density has been observed to vary with climate, vegetation, relief and soil and rock properties (Tucker et al., 2001b; Luo et al., 2016). Several analytical models have been proposed to explain drainage density and the closely related metric valley spacing (Montgomery and Dietrich, 1992; Howard, 1997; Perron et al., 2008, 2009, 2012). In most of these models streamflow scales with drainage area, and the flow paths of water towards streams and the processes generating streamflow are

20 not specified. However, several studies have suggested that groundwater flow plays an important role in controlling streamflow and drainage density (Carlston, 1963; de Vries, 1994; Dunne, 1990; Twidale, 2004). Direct erosion by groundwater discharge, also termed seepage erosion, and its effect on the initiation and development of channel networks has been explored extensively (Dunne, 1990; Pederson, 2001; Abrams et al., 2009; Brocard et al., 2011). However, apart from direct erosion, groundwater

also has an indirect effect on erosion by contributing to streamflow and by controlling the watertable, which in turn affects the
storage available in the unsaturated zone and the magnitude and spatial distribution of saturation overland flow (Dunne and
Black, 1970; Freeze, 1972; de Vries, 1976).

A number of analyses of river networks have noted a relation between drainage density, lithology and transmissivity (Carlston, 1963; Luo and Stepinski, 2008; Bloomfield et al., 2011). Drainage density has been used infer the transmissivity and permeability of the subsurface (Luo et al., 2010; Luo and Pederson, 2012; Bresciani et al., 2016). A review of drainage density in the conterminous USA found a relation with independent data on subsurface permeability (Luo et al., 2016). These studies imply that a relation exists between permeability, groundwater flow and drainage density. However, to my knowledge a causal mechanism for this relation has not been proposed.

Most numerical landscape models use simplified representations of groundwater flow, and do not simulate the watertable or lateral groundwater flow directly (Tucker et al., 2001a; Bogaart et al., 2003; van der Meij et al., 2018). There are some exceptions, including two case studies of single river catchments (Huang and Niemann, 2006; Barkwith et al., 2015) and a generic model study (Zhang et al., 2016), that concluded that the inclusion of groundwater flow has a strong effect on modelled relief and erosion rates. Recently, a groundwater flow component has been added to the landscape evolution model code Landlab (Litwin et al., 2020). However, to my knowledge there has been no systematic model study to explore the relation between groundwater flow and drainage density.

Here, I present a new coupled model of groundwater flow, overland flow and erosion. The model was inspired by the coupled groundwater and streamflow model of de Vries (1994). The model includes lateral groundwater flow, the watertable and its effect on the partitioning of groundwater and overland flow and erosion processes that follow widely-used equations (Tucker and Hancock, 2010). The model is used to explore the sensitivity of drainage density to parameters that govern groundwater flow, stream flow and erosion. The results point to a strong relation between drainage density, groundwater flow and transmissivity. In addition, the results illustrate the process of groundwater capture that explains this relation.

2 Methods

2.1 Model description

The model code described here simulates steady-state groundwater flow, transient saturation overland flow, stream incision and hillslope diffusion in a two-dimensional cross-section of the subsurface. These processes are shown schematically in Fig. 1. The model code is named the groundwater flow, overland flow and erosion model, or GOEMod, and was inspired by the conceptual groundwater outcrop erosion model originally presented by de Vries (1976) and subsequently implemented as a set of coupled analytical solutions for groundwater and streamflow (de Vries, 1994). GOEMod is an open source code and is available online on Zenodo (Luijendijk, 2021) and GitHub (https://github.com/ElcoLuijendijk/goemod).

Groundwater flow is approximated as steady-state, with the dark blue line in Fig. 1 showing the average groundwater level. Each precipitation event adds a volume of water on top of the average groundwater level, shown by a light blue area. Saturation overland flow occurs where the groundwater level is so close to the surface that there is no storage space available in the

unsaturated zone. Note that infiltration-excess overland flow is included in the model code, but is not used in this study, because of the focus on humid regions where infiltration excess overland flow is of minor importance (Dunne, 1978; Bogaart et al., 2003). Groundwater flow and saturation overland flow contribute to steady-state and transient streamflow, respectively.

60   Both components of streamflow lead to erosion and incision of the stream. In addition, the areas outside streams erode by hillslope diffusion, which is a simplified representation of processes such as soil creep (Culling, 1960, 1963).

The model starts with a rectangular model domain with a constant slope in one direction. The rectangular model domain contains a single cross-section that is oriented perpendicular to the slope and that is used to solve the groundwater flow, overland flow and the hillslope diffusion equations. The initial topography in the direction of the cross-section is randomly perturbed.

65   The topography evolves over time as a result of stream incision and hillslope diffusion. The model simulates groundwater flow, overland flow and hillslope diffusion in the 2D cross-section. All streams are assumed to run perpendicular to the cross-section and are perfectly straight and parallel. Streamflow and stream incision are calculated by multiplying the water and sediment flux in the 2D cross-section with the contributing area perpendicular to the cross-section. The resulting model is 2.5D in the sense that it simulates water fluxes and incision of a series of perfectly parallel streams that develop along an inclined topography.

70   The workflow and equations for each component of the model are discussed in detail in the following sections.
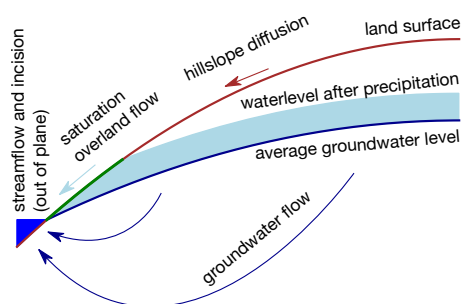
Figure 1. Conceptual model showing the hydrological and erosion process represented in the new model code. The hydrological processes include groundwater flow, overland flow and streamflow. The erosion processes include hillslope diffusion and stream incision.

2.2   Initial topography

The model starts with a random initial topography, which is calculated as using a series of 200 linear segments with random placement and random perturbation of the elevation at the start and end points of the segments. For the model simulations shown in this study, the average initial elevation is 0 m and the initial relief is 0.5 m.

2.3 Partitioning of groundwater and overland flow

The subdivision of precipitation between evapotranspiration, overland flow and groundwater flow in the model is calculated for individual precipitation evens. For each precipitation event groundwater recharge is assumed to equal the available storage in the unsaturated zone, i.e., all groundwater stored in the unsaturated zone is assumed to eventually percolate to the groundwater table. For each point in the model domain the available storage in the unsaturated zone is calculated using the depth of the watertable and the specific yield of the subsurface as:

$$s = S_y(z - h) \tag{1}$$

where s is storage (m), S_y is specific yield (dimensionless), z is the elevation of the land surface (m) and h is the elevation of the watertable (m). Groundwater recharge for a single precipitation event is calculated as:

$$R_i = \begin{cases} s & \text{if } s < P_d \\ P_d & \text{if } s >= P_d \end{cases} \tag{2}$$

where P_d is precipitation depth per event (m), R_i is groundwater recharge depth per event (m),

The time-averaged potential recharge rate $\overline{R_p}$ ($\mathrm{m\,s^{-1}}$) is calculated as the sum of the individual recharge events as:

$$\overline{R_p} = \left(\sum_{i=11}^{i=n} (R_i f_i) \right) / \Delta t_r \tag{3}$$

where f_i is the frequency of precipitation event i ($\mathrm{a^{-1}}$), and Δt_r is the duration of the reference time period, which is one year (s). The actual recharge rate is calculate by subtracting evapotranspiration:

$$R = \begin{cases} R_p - ET & \text{if } R_p > ET \\ 0 & \text{if } R_p \leq ET \end{cases} \tag{4}$$

where ET is the evapotranspiration rate ($\mathrm{m\,s^{-1}}$). Note that for simplicity the evapotranspiration rate is assumed to be constant and independent of the depth of the watertable.

Saturation overland flow is calculated as the amount of precipitation that exceeds the available storage (s) in the unsaturated zone. For each node in the model domain and for each precipitation event the saturation overland flow depth is calculated as:

$$Q_{si} = \begin{cases} P_d - S & \text{if } s < P_d \\ 0 & \text{if } s >= P_d \end{cases} \tag{5}$$

where Q_{si} is the saturation overland flow depth per precipitation event (m).

2.4 Precipitation

Precipitation events are quantified using rainfall intensity statistics for the Netherlands (Beersma et al., 2019), using a precipitation-frequency curve shown in Figure 2. The rainfall-intensity curves follow a generalized extreme value distribution with the parameters given by the following equations (Beersma et al., 2019),:

$$\eta = 1.02\,(0.239 - 0.0250\log(D/60.))^{-1/0.512} \tag{6}$$

$$\gamma = 0.478 - 0.0681\log(D) \tag{7}$$

$$\kappa = 0.118 - 0.266\log(D) + 0.0586(\log(D)^2) \tag{8}$$

where η is the location parameter, γ is the dispersion parameter and κ is the shape parameter of the distribution and D is the duration of each rainfall event (s). For the model experiments shown in this study a rainfall duration (D) of 3 hours is used. The precipitation depth for a single precipitation event is calculated as:

$$P_d = 1000.0\eta\left(1.0 + \gamma/\kappa(1.0 - T^{-\kappa})\right) \tag{9}$$

where P_d is the rainfall depth per event (m) and T is repetition time (a), which is the reciprocal of precipitation frequency f (a^{-1}). The model simulates overland flow and groundwater recharge for an average year. The total number of precipitation events in a single year is found by adding up a series of precipitation events until the sum of the individual events matches a desired volume for the total annual precipitation (P_t):

$$P_t = \sum_{i=f_1}^{i=f_2}\left(P_d(i)f(i)\right) \tag{10}$$

The precipitation events per year are calculated starting with a frequency (f_1) of 1 a^{-1}. Subsequently higher frequency (and lower magnitude) events are added progressively until the desired amount of total precipitation per year is reached. The precipitation statistics are based on an average humid climate such as the Netherlands, with a total precipitation (P_t) of 0.75 m a^{-1}.

2.5 Groundwater flow

The model is based on the assumption that groundwater flow can be considered to be in steady-state on the timescales of stream and hillslope erosion processes. This was judged to be reasonable because the groundwater flow system reacts much
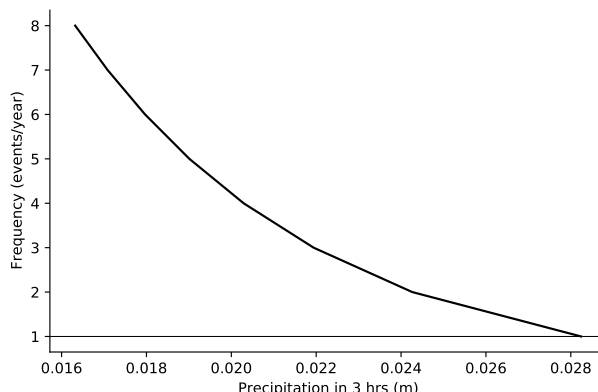
Figure 2. Precipitation frequency curve for the Netherlands, following Beersma et al. (2019) for precipitation events with a duration of three hours. This curve was used to model precipitation, groundwater recharge and overland flow.

faster than the relatively slow rates of erosion. Given these assumptions, groundwater flow and the position of the watertable can be calculated using analytical solutions of steady-state groundwater flow.

First, the out of plane component of groundwater flow, i.e., groundwater flow parallel to the direction of the nearest stream, is calculated using Darcy's equation and assuming the out of plane hydraulic gradient is equal to the (out-of-plane) slope of the nearest stream:

$$Q_{go} = TS \tag{11}$$

where T is transmissivity ($\mathrm{m^2\,s^{-1}}$), and S is stream slope ($\mathrm{m\,m^{-1}}$). Out of plane groundwater flow can be significant for cases with high transmissivity or stream slope, as shown in Fig. 3.

The remaining in-plane groundwater flow (i.e., towards the nearest stream) is calculated using the value of recharge calculated in equation 3 and subtracting the out-of-plane discharge:

$$R_e = \overline{R}L_u - Q_{go} \tag{12}$$

where R_e is the effective in-plane recharge $\mathrm{m\,s^{-1}}$, and L_u is the length of the upstream contributing area m.

In-plane groundwater flow is calculated using the Dupuit-Forchheimer equation, which describes depth-integrated, steady-state groundwater flow between two groundwater discharge points (Forchheimer, 1886; Bresciani et al., 2016):

$$\Delta h = \frac{\overline{R_e}}{T}x(L-x) + \Delta Hx/L \tag{13}$$

where h is hydraulic head (m), L is the distance between two groundwater discharge points (m), x is the distance to the first discharge point (m) and ΔH is the difference in water level between the two discharge points (m). The term groundwater

Earth **Surface**
Dynamics
Discussions
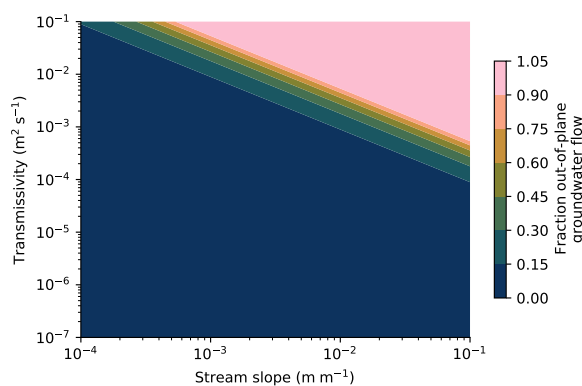
Figure 3. Calculated out-of-plane groundwater flow for a range of values of transmissivity and stream slope, and using the base-case values of contributing area (5 km) and groundwater recharge ($0.375 \ \mathrm{m \ a^{-1}}$).

discharge point represents a point such as a stream or a part of the land surface where the watertable is at the surface and where groundwater seepage takes place. The equation assumes that the lateral differences in hydraulic head (h) are much smaller than the thickness of the aquifer (Bresciani et al., 2016).

140   For points at the edge of the model domain that are only bound by a discharge point on one side, the equation reduces to:

$$\Delta h = \frac{\overline{R_e}}{T} x (L_b - x) \tag{14}$$

Where L_b is the distance between the discharge point and the downstream model boundary (m). The average in-plane groundwater recharge rate $\overline{R_e}$ was calculated as the average effective recharge rate for all the nodes in between two seepage nodes. The seepage nodes represent points where the watertable is at the surface and where groundwater discharge occurs. The
145   position of the seepage nodes is not known in advance, but is calculated using the following iterative procedure:

1. First one seepage node is picked at the lowest elevation in the model domain and the watertable is calculated using equations 13 and 14. In most cases the calculated watertable is still above the land surface in a large part of the model domain after the first iteration.

2. Subsequently a new seepage node is added at the node with the lowest elevation in the part of the model domain where
150   the modelled watertable exceeds the land surface.

3. The watertable is recalculated using this new additional seepage node.

4. The last two steps are repeated until the modelled watertable is below or at the land surface (i.e., $h \leq z$) everywhere.

An example of the calculated watertable and seepage locations following the procedure is shown in Fig. 4.
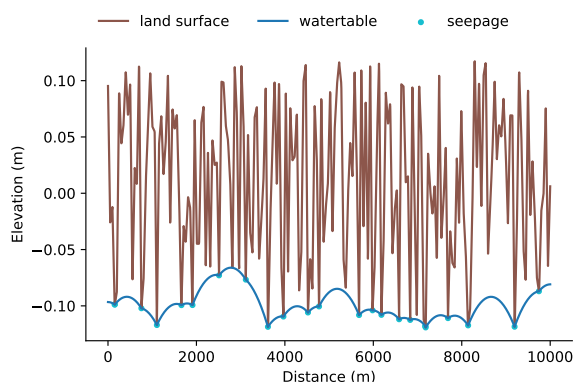
Figure 4. Example of initial topography and calculated watertable and groundwater seepage locations. The watertable and seepage locations were calculated by an iterative solution of eqs. 13 and 14 as explained in section 2.5.

2.6 Stream flow

155 The water flow in each stream consists of two components, steady baseflow supplied by groundwater discharge, and transient flow that consists of overland flow. The calculation of both components is described in the following two sections:

2.6.1 Baseflow

The baseflow in each stream node is calculated in two steps. First, streams nodes are found by finding the node with the lowest elevation for each series of neighbouring seepage nodes in the model domain. Note that the term seepage nodes is used here

160 to denote nodes where groundwater discharge occurs. The two-dimensional (in-plane) value of groundwater flow toward each stream node (q_b) is calculated for each stream by finding the nodes contributing groundwater to each stream and by summing the product of the recharge rate at each node R and the width of each node (Δx). The contributing area is found using the taking the watertable h as calculated using equations 13 and 14 and finding the two nodes on either side of each stream where the hydraulic gradient changes direction. The three dimensional (out of plane) value of baseflow was calculated by multiplying

165 in-plane baseflow (q_b) with an upstream length of each stream:

$$Q_b = q_b L_u \qquad (15)$$

where Q_b is baseflow. An example of the calculate value of baseflow is shown in Fig. 5.
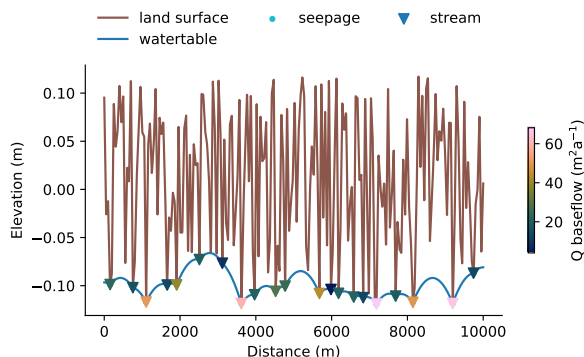
Figure 5. Example of calculated baseflow to streams.

2.6.2 Saturation overland flow

The volume of water that is contributing to overland flow is calculated per precipitation event as:

$$V_0 = \int_{x1}^{x2} Q_{si} dx \tag{16}$$

170

Where V_0 is the volume of water to be discharged in a stream channel ($\mathrm{m^3}$), x_1 and x_2 are the position of the topographic divide on either side of the channel (m) and Q_{si} is the rate of overland flow for each node as calculated using equation 5. An example of the resulting distribution of precipitation excess and overland flow is shown in Fig. 6.

2.6.3 Waterlevel in streams

175 The waterlevel in streams as a result of baseflow and overland flow is calculated using the Gauckler-Manning equation for stream discharge. The Gauckler-Manning equation for stream discharge is (Gauckler, 1867; Manning, 1891):

$$v = K_n R^{2/3} S^{1/2} \tag{17}$$

where v is the mean flow velocity in a stream channel ($\mathrm{m\,s^{-1}}$), K_n is an empirical coefficient ($\mathrm{m^{1/3}s^{-1}}$), which is defined as $1/n$ where n is Manning's roughness coefficient ($\mathrm{s\,m^{-1/3}}$), R is hydraulic radius (m) and S is the slope of the water surface, 180 which is taken as equal to the slope of the channel bed ($\mathrm{m\,m^{-1}}$). With the common assumption that channels are much wider than deep, $R \approx h_c$ and the equation can be simplified to:

$$v = K_n S^{1/2} h_c^{2/3} \tag{18}$$
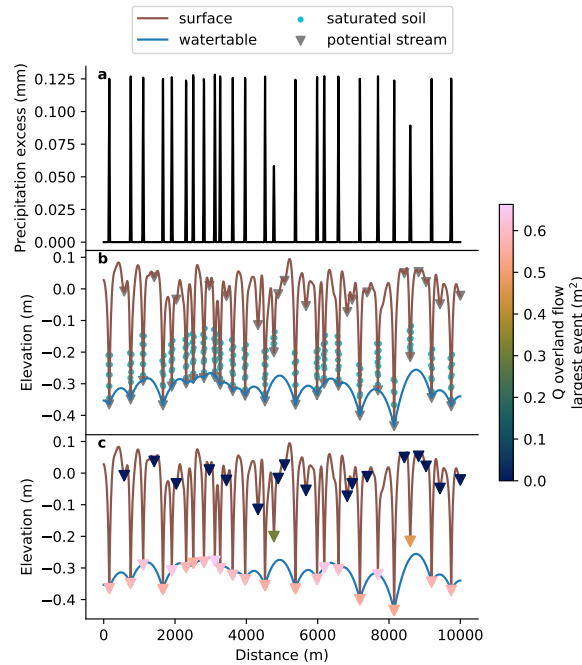
Figure 6. Example of calculated precipitation excess and saturation overland flow in streams. Panel a shows the calculated precipitation excess for each node in the model domain. Panel b shows the location of nodes where the precipitation depth for a single event exceeds the available storage, which results in fully saturated conditions and the generation of saturation overland flow. Panel c shows the calculated saturation overland flow volume for each stream in the model domain. Note that all the potential streams are shown here, including potential streams in depressions that do not generate overland flow because they are located too far above the watertable.

where h_c is the water height in the channel (m). The discharge is equal to the product of the flow velocity and the cross-sectional area. To simplify the equations the cross-section for each stream is assumed to be triangular. The linear in-plane slope of the channel bed (i.e., perpendicular to the flow direction in the channel) is denoted as S_t (m m^{-1}). The cross sectional area A of the channel equals $S_t h^2$. Using this the discharge equation can be written as:

$$Q_w = \frac{K_n S^{1/2}}{S_t} h_c^{8/3} \tag{19}$$

where Q_w is the discharge in the channel (m^{3}s^{-1}) and $C_2 = \frac{K_n S^{1/2}}{S_t}$. Rewriting this equation yields and expression for the waterlevel in streams as a function of discharge:

$$h_c = \left(\frac{S_t Q_w}{K_n S^{1/2}} \right)^{3/8} \tag{20}$$

Earth **Surface**
Dynamics
Discussions

2.6.4 Transient stream discharge

The discharge generated by overland flow operates on short timescales of hours to days. Modelling this process directly would require short timesteps that would make the model prohibitive computational expensive. Instead here I derive new equations for the discharge over time and the total discharge in a stream following a single precipitation event. To keep the solution

195 mathematically tractable the assumption is made that each precipitation event generates a volume of overland flow that is added instantaneously to the stream channel. The volume is subsequently discharged over time.

The continuity equation for discharge of a stream channel is given by:

$$\frac{\partial V_w}{\partial t} = -Q_w \tag{21}$$

where V_w is the water volume in the channel (m^3). We define the volume to be discharged as the product of a cross-sectional

200 area that changes over time and a fixed stream length L_u (m):

$$V_w = AL_u \tag{22}$$

assuming that the shape of the channel is a triangle and combination with the stream discharge equation (eq. 19) yields:

$$\frac{L_u}{S_t}\frac{\partial h_c^2}{\partial t} = -\frac{K_n S^{1/2}}{S_t}h_c^{8/3} \tag{23}$$

Integration of this equation with boundary condition $h_c = h_0$ at $t = 0$ yields:

205 $$h_c = \left(h_0^{-2/3} + \frac{K_n S^{1/2}}{3L}t\right)^{-3/2} \tag{24}$$

The initial heigh of the waterlevel in the channel (h_0) is related to the initial volume of water in the channel V_0:

$$V_0 = \frac{h_0^2 L_u}{S_t} \tag{25}$$

Adding eq. 25 into eq. 24 and replacing the constants yields an expression for the decrease of waterlevel in a channel over time in response to drainage of an initial volume V_0:

210 $$h_c = \left(\frac{V_0 S_t}{L_u}^{-1/3} + \frac{K_n S^{1/2}}{3L_u}t\right)^{-3/2} \tag{26}$$

This equation was validated by comparison with a numerical solution of for the waterlevel over time (Fig. 7). The numerical solution was calculated using the discharge equation (eq. 19) to calculate discharge over time. At the first timestep the initial

Earth **Surface**
Dynamics
Discussions
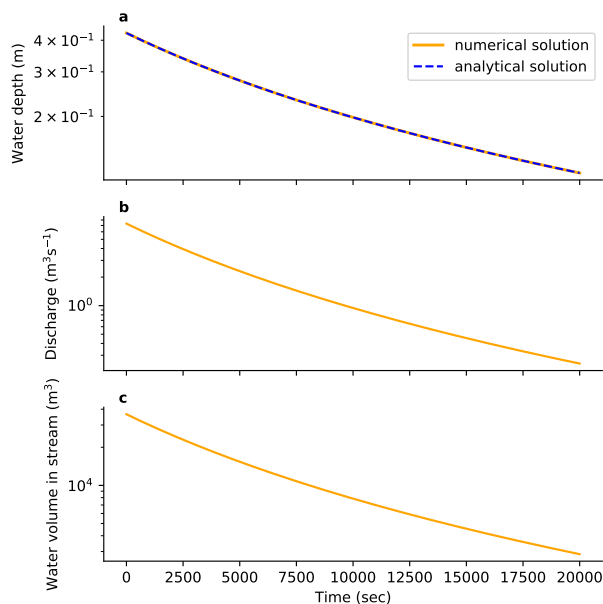
Figure 7. Validation of the equation for the transient discharge of an instantaneously added volume of water in a stream channel (eq. 26) using the numerical solution as described in the text. Panel a shows that the numerical solution and analytical solution overlap perfectly. Panel b and c show the change in water volume and discharge in the channel over time, which were used to calculate the numerical solution in panel a. The solution uses base case parameters listed in Table 1, a precipitation depth of 0.0365 m, which is the theoretical maximum 1-day precipitation depth for a return time of 1 year for the Netherlands, and a contributing area for overland flow with a length of 100 m.

overland flow volume V_0 is added. Subsequently discharge is calculated and subtracted from the initial volume V_0. The heigh of the waterlevel at each timestep was calculated using equation 25. This process is repeated until the waterlevel is less than 1

215   mm.

2.7   Stream incision

The sediment flux in a stream channel at carrying capacity is given by (Tucker and Bras, 1998; Tucker and Hancock, 2010):

$$Q_s = wk_f(Q_w/w)^m S^n \qquad (27)$$

where Q_s is the sediment flux m^3s^{-1}, w is channel width (m), k_f is the sediment transport coefficient (dimensionless), Q_w

220   is water discharge $(m^{-3}s^{-1})$, S is channel slope (dimensionless) and m is the discharge exponent (dimensionless) and n is the slope exponent (dimensionless). The erosion by streams is subdivided into two components, the erosion by baseflow driven by groundwater discharge and the additional transient erosion by saturation overland flow during and directly after precipitation events. The equations for these two erosion components are discussed in the following sections.

Note that the incision of streams results in an adjustment of the stream slope (S). The initial value of stream slope is fixed.
225   After each timestep a new value of stream slope is calculated using the new elevation of the base of the stream, and the elevation of the downstream edge of the model domain, which is assumed not to change over time:

$$S = \frac{z_s - z_b}{L_d} \tag{28}$$

where z_s is the elevation fo the stream in the modelled cross-section (m), z_b is the elevation of the downstream model boundary (m), and L_d is the distance to the downstream model boundary (m). The elevation of the downstream boundary does
230   not change over time and is the product of the initial slope (S_0) and L_d.

2.7.1   Stream incision by baseflow

The sediment flux in the steam channel carried by baseflow is calculated using equation 27 and using the value of baseflow calculated using equation 15 as the value for water discharge Q_w. The incision of the stream is calculated by dividing the sediment flux by the channel width (w). In addition, the erosion is divided over the upstream length of the stream by assuming
235   that erosion increases linearly from zero at the start of the stream to the maximum value at the end of the stream. This yields the following equation for erosion of the stream channel:

$$\frac{\partial z}{\partial t} = (1 - \phi) \frac{Q_s}{w \frac{1}{2} L_u} \tag{29}$$

where z is the elevation of the base of the channel (m), t is time (sec), ϕ is porosity (dimensionless). Note that the linear increase of erosion by baseflow along the stream is a simplification that makes the problem more tractable mathematically. In
240   reality the non-linear relation between streamflow and erosion would result in a non-linear increase in erosion along the stream profile.

Channel width was calculated as (Lacey, 1930):

$$w = k_w Q^\omega \tag{30}$$

where k_w and ω are empirical parameters. We use values of $k_w = 3.65$ and $\omega = 0.5$ (van den Berg, 1995).

245   ### 2.7.2   Stream incision by overland flow

The erosion by streams caused by the discharge of overland flow is calculated by combining the equation for stream discharge due to overland flow over time (eq. 26) with the sediment discharge equation (eq. 27). The combination of these two equations yields:

$$Q_s = k_f S^n \left(\frac{K_n S^{1/2}}{S_t} \right)^m \left(\left(\frac{V_0 S_t}{L_u} \right)^{-1/3} + \frac{K_n S^{1/2}}{3 L_u} t \right)^{-4m} \tag{31}$$

250   Integrating this equation from $t = 0$ to $t = \infty$ yields an expression for the total volume of sediment eroded from the channel after a single precipitation and discharge event:

$$V_s = \frac{a(b+c)^{(-4m+1)}}{4mc+c} \tag{32}$$

where V_s is the total volume eroded in a stream by overland flow following a single precipitation event, a, b and c are constants that are defined as:

255    $$a = k_f S^n \left(\frac{K_n S^{1/2}}{S_t} \right)^m \tag{33}$$

$$b = \left(\frac{V_0 S_t}{L_u} \right)^{-1/3} \tag{34}$$

$$c = \frac{K_n S^{1/2}}{3L_u} \tag{35}$$

The eroded volume results in incision of the stream. Stream incision by overland flow is calculated by distributing the eroded volume (V_s) evenly over the width of the stream channel (w). In addition, erosion by overland flow is assumed to 260   increase linearly from the start of the channel to the position of the modelled cross-section. This is a similar simplifcation as the linear increase of erosion by baseflow discussed in the previous section, and was likewise also used to keep the problem mathematically tractable. This yields the following expression for the incision of the stream due to overland flow:

$$\Delta z_s = \frac{V_s}{(w\frac{1}{2}L_u)} \tag{36}$$

where Δz_s is stream incision following a single precipitation event (m).

265   **2.8   Hillslope diffusion**

Erosion of the parts of the model domain outside of the streams follows the hillslope diffusion equation (Culling, 1960):

$$\frac{\partial z}{\partial t} = \frac{\partial \left(K_d \frac{\partial z}{\partial x} \right)}{\partial x} \tag{37}$$

Where K_d is the hillslope diffusion coefficient ($m^2\,s^{-1}$). This equation was solved numerically using a standard implicit finite difference approach using a matrix solver implemented in the Python module Numpy (Harris et al., 2020).

270   **2.9   Iterative solution**

The solution of the equations for groundwater flow, overland flow, streamflow and erosion follow an iterative scheme that is detailed in Fig. 8. After setting up an initial topography, the initial watertable is calculated using the procedure described in
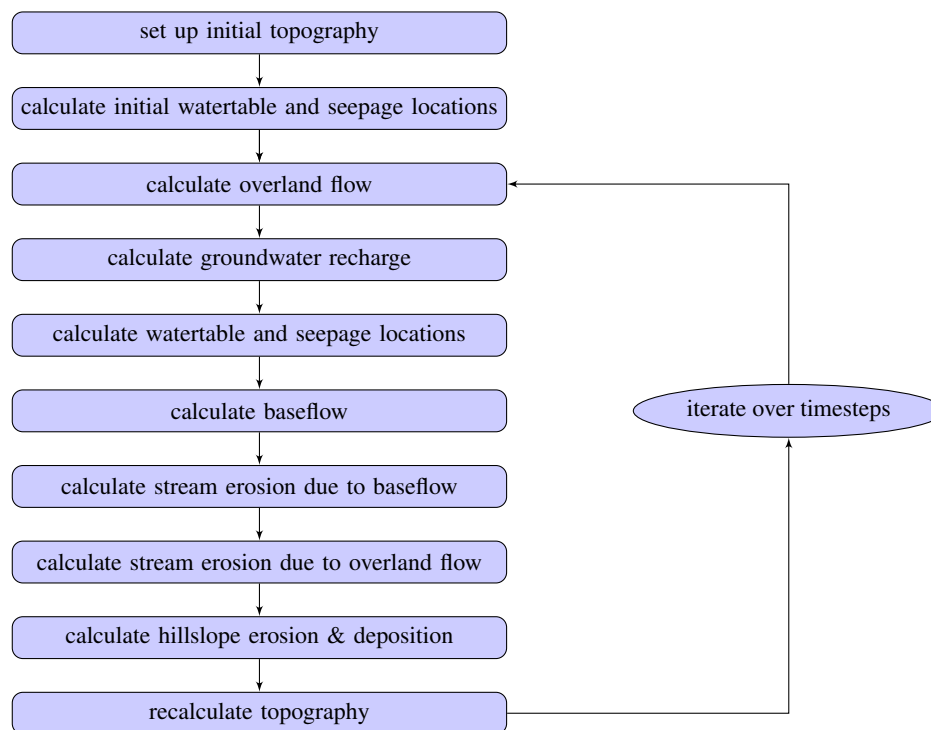
Figure 8. Flowchart for the iterative solution of the groundwater flow, overland flow and erosion equations

section 2.5, with recharge taken as the difference between the total precipitation (P_t), overland flow and evapotranspiration (ET). Subsequently the model calculates baseflow, stream incision due to baseflow and overland flow, and topography change

275 due to hillslope diffusion. The procedure is repeated at each timestep. The initial timestep size is 1 year. The timestep size is was adjusted so that the maximum elevation change per timestep was 0.5% of the total relief with a minimum of 0.01 m. These conditions were found by trail and error to ensure numerically stable and computationally efficient model runs for the range of parameter values and runs reported in this study.

2.10 Base case parameter values

280 The base case parameter values follow Bogaart et al. (2003) who modelled stream network and landscape evolution for north-western Europe under alternating glacial and interglacial conditions. Here the parameters that represent present-day (inter-glacial) conditions are used. The base case parameters are listed in table 1. In contrast to the relatively high value for porosity of 0.4 used by Bogaart et al. (2003) here a value of 0.2 is used that more closely follows values observed in areas covered by fluvial and aeolian sediments in the southern Netherlands (de Vries, 1994). The base case value for transmissivity is 1×10^{-3}

285 $\mathrm{m^2 s^{-1}}$, which is lower than values of 0.012 to 0.03 $\mathrm{m^2 s^{-1}}$ reported by de Vries (1994). The relatively low value of transmissivity was chosen because higher values led to a very low drainage densities, which made them less suitable as a starting point for sensitivity analyses. For initial slope a value of 5×10^{-3} was chosen, which is higher than the average stream gradient in

the Netherlands of 5×10^{-4} m m^{-1}. Lower values resulted in models where channel initiation was so slow that the modelled drainage density reflected the initial random topography, as will be further discussed in section 4.1.

Table 1. Base case parameter values

parameter group	parameter name	symbol	value	reference
Model geometry	length	L	10000 m	
	upstream length	L_u	5000 m	
	downstream length	L_d	5000 m	
	grid cell size	Δx	5 m	
Relief	initial relief		0.5 m	
Precipitation and ET	precipitation event duration	D	1.0 day	
	annual precipitation	P	0.75 m a^{-1}	Bogaart et al. (2003)
	potential ET	ET	0.375 m a^{-1}	Bogaart et al. (2003)
Stream flow	channel roughness factor	K_n	25	de Vries (1994)
	initial channel slope	S_0	5×10^{-3}	
	perpendicular channel slope	S_t	0.05	
	channel width coefficient 1	k_w	3.65	van den Berg (1995)
	channel width coefficient 2	ω	0.5	van den Berg (1995)
Groundwater flow	specific yield	S_y	0.2	
	transmissivity	T	1×10^{-3} m^2 s^{-1}	
Erosion	sediment transport coefficient	k_f	0.32	Tucker and Bras (1998)
	discharge exponent	m	1.8	Bogaart et al. (2003)
	slope exponent	n	2.1	Bogaart et al. (2003)
	hillslope diffusion coefficient	K_d	0.01 a^{-1}	Bogaart et al. (2003)
	porosity	ϕ	0.2	

2.11 Model sensitivity analyses

To explore the role of groundwater flow in erosion a series of model experiments were conducted with different values for transmissivity and specific yield. To compare the effects of changes in groundwater flow with climate and erosion parameters, an additional set of experiments was conducted with different values for total precipitation (P_t), hillslope diffusion coefficient (K_d) and slope exponent (n). These values are listed in table 2.

The range of variation of the hillslope diffusion coefficient was based on Richardson et al. (2019). There are no large compilation of transmissivity available. Models and data of the permeability of unconsolidated sediments (Gleeson et al., 2011; Luijendijk and Gleeson, 2015) and an hydrologically active layer of approximately 100 m (Gleeson et al., 2016; Jasechko et al.,

2017) suggests a variation of approximately 10^{-7} to 10^{-1} $\mathrm{m^2\,s^{-1}}$. Here a smaller range of values is evaluated, 10^{-4} m to 10^{-1} m, because lower values result in drainage densities that are fully controlled by the initial random topography. The values of

300 specific yield are based on values reported for mixed sediments (Revil, 2002; Gleeson et al., 2014; El-husseiny, 2020). The variation of the slope exponent was based on a global compilation by Harel et al. (2016).

Table 2. Parameter value range in model sensitivity analyses

parameter name	symbol	value, minimum	value, maximum
precipitation	P	$0.5\ \mathrm{m\,a^{-1}}$	$1.0\ \mathrm{m\,a^{-1}}$
transmissivity	T	1×10^{-5} m	1×10^{-1} m
specific yield	S_y	0.15	0.5
hillslope diffusion coefficient	K_d	$4 \times 10^{-5}\ \mathrm{m^2\,a^{-1}}$	$4 \times 10^{-2}\ \mathrm{m^2\,a^{-1}}$
stream slope	S	1×10^{-4}	0.025
slope exponent	n	1.0	2.6

3 Results

3.1 Groundwater capture

Figure 9 shows the result of an example model run using the base case parameters values as shown in Table 1. The figure shows
the evolution of the land surface from an initial randomly generated surface over a timespan of 100,000 years. The system starts
out with a very high drainage density, with 65 streams. Subsequently the model evolves towards a system dominated by fewer
streams over time, with the final number of 13 active streams after a runtime of 100,000 years.

The decrease in number of streams is caused by a process that is referred to here as groundwater capture, by which faster
eroding streams draw the watertable below neighbouring streams and reduce the baseflow and saturation overland flow of these
streams until they fall dry. The process of groundwater catchment capture is illustrated in more detail in Figure 10, which shows
the land surface, watertable and stream fluxes for three timeslices before, during and after a groundwater catchment capture
event. After 73 kyr (Fig. 10a) there are still 15 streams that are active. However, the second stream from the left hand side has
smaller catchment area and a lower baseflow, and therefore incises slower than its two neighbouring streams. After 79 kyr (Fig.
10b) the neighbouring streams have incised further and have drawn the watertable below the base of the stream. The second
stream does generate overland flow, but has ceased to generate baseflow. At 86 kyr the watertable has been drawn down further
and the watertable is too deep for the second stream to generate saturation overland flow, i.e., all the precipitation that falls near
the stream can be accommodated in the unsaturated zone above the watertable. As a results the stream has become inactive.
The stream channel has partly been filled by hillslope diffusion, because the sediment flux caused by hillslope diffusion is no
longer compensated by the removal of sediment by streamflow.

The evolution of the stream network over time is summarized in Figure 11. Initially each small depression is potentially
an active stream channel, which results in a large number of active streams. However as the incision of streams increases the
number of active streams drops rapidly in the first 15 kyr, followed by a slower reduction in the number of active streams
for the remainder of the model run. The continuing incision and the reduction of active streams by groundwater capture also
means that the area susceptible to saturation overland flow decreases over time, because saturation overland flow takes place
near active stream channels where the watertable is located close to the surface. Apart from a short phase at the start of the
model run streamflow and stream erosion are predominantly generated by groundwater flow, which is named baseflow once it
enters the stream channel (Fig. 11b, c).
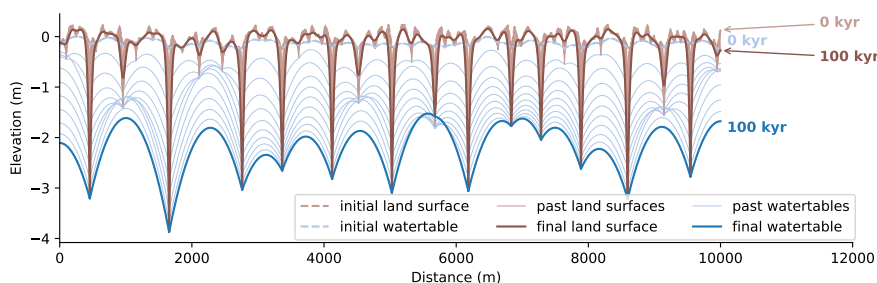
Figure 9. Modelled change in land surface and watertable over 100,000 years for the base case model run. The results show the evolution from a random topography to a system with 13 active streams. The past positions of the land surface and watertable show that the number of active streams decreased over time. The time between each past watertable position that is shown is 10,000 years.
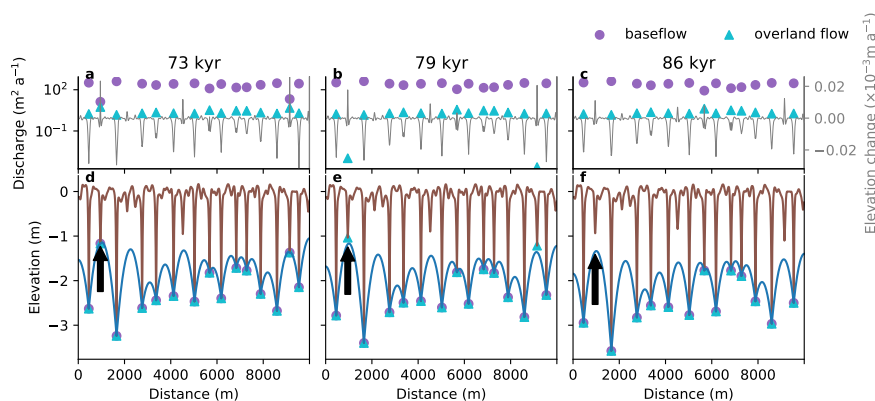
Figure 10. Illustration of groundwater capture in the base case model run. Panel a, b, c show modelled streamflow generated by baseflow and overland flow, and the change in elevation caused by hillslope diffusion and stream erosion for three timeslices before, during and after a capture event, respectively. Panels d, e and f show the modelled position of the land surface and the watertable during these three timeslices. The arrow points to the stream that loses its connection to the groundwater table.

Earth **Surface**
Dynamics
Discussions
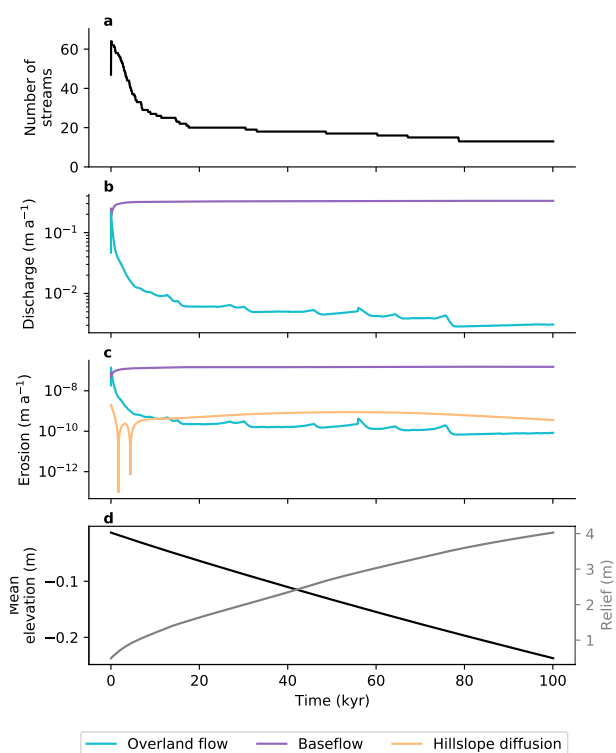
Figure 11. Changes in drainage density (panels a), water discharge (panel b), sediment flux (panels c) elevation and relief (panels d) over time for the base-case model run. The results show a decrease of active stream channels and a decrease in saturation-excess overland flow over time as streams incise and the watertable is drawn deeper below the land surface.

3.2 Sensitivity of drainage density to transmissivity

Groundwater capture is dependent on the transmissivity of the subsurface. This is illustrated by three model runs with different

330 values of transmissivity (Fig. 12). The model run with the lowest transmissivity shows the higher drainage density (Fig. 12a) and a model run with a high value of transmissivity shows a low value of drainage density ((Fig. 12c). The reason is that a low transmissivity results in higher watertable gradients, which makes it much more difficult for streams to draw the watertable below neighbouring streams and to capture their groundwater discharge. In contrast, high transmissivity results in a relatively flat watertable, which means that small differences in incision can already lead to a watertable that is drawn below the base

335 of streams. There is a small positive correlation between transmissivity and stream incision rate. The lower number of streams at high values of transmissivity means that these streams receive more water and therefore have a higher erosion power. However, at high transmissivity the groundwater flow direction also changes and the proportion of out-of-plane groundwater flow increases (Fig. 3). This results in a lower in-plane groundwater flow toward streams and lower incision rates at high transmissivities. These two mechanisms compete with each other. At transmissivities exceeding $10^{-2.0}$ m^2 s^{-1} the increase in

340 out-of-plane groundwater flow becomes dominant and results in a decrease in incision rate (Fig. 13).

Earth **Surface**
Dynamics
Discussions
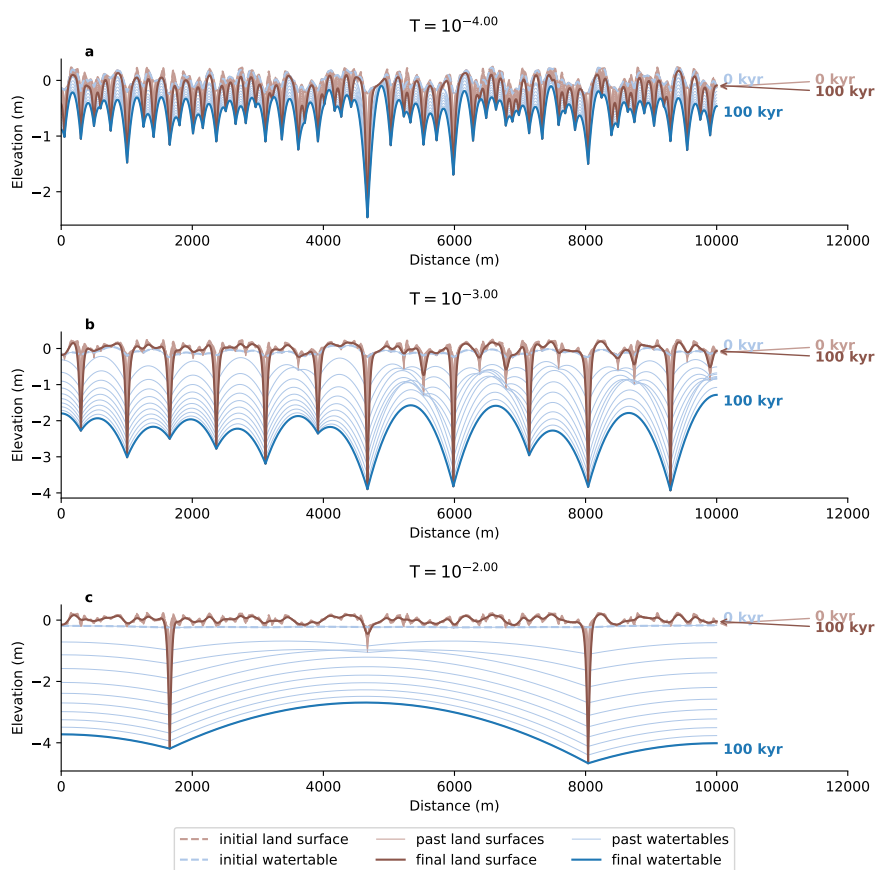
Figure 12. Modelled change in land surface and watertable over time for three model experiments with low ($T = 10^{-4}$ m^{2}s^{-1}, panel a), moderate ($T = 10^{-3}$ m^{2}s^{-1}, panel b) and high ($T = 10^{-2}$ m^{2}s^{-1}, panel c) transmissivity. The results show a negative correlation between drainage density and transmissivity and a positive correlation between transmissivity and stream incision over the model runtime of 100,000 years.

3.3 Sensitivity of drainage density to hydrological and erosion parameters

Comparison of drainage density and incision to a number of parameters that govern erosion and streamflow show that drainage density is the most sensitive to transmissivity, followed by stream slope and slope exponent (Fig. 13). Drainage density is positively correlated with slope exponent, hillslope diffusion coefficient and precipitation, and is negatively correlated with transmissivity and initial stream slope.

The strong negative correlation of drainage density and initial downstream slope is illustrated in Fig. 14 and can be explained by two effects. First, higher stream slope means that individual streams have a higher incision power, which means that it is easier to draw the watertable below adjacent streams and capture their groundwater discharge. Second, a higher initial downstream slope means that more of the total groundwater recharge is directed downstream in the out-of-plane direction, and there is less in-plane groundwater flow (Fig 3). This results in flatter watertables and an increase in groundwater capture. The slope exponent results in similar magnitude of changes in drainage density and stream incision (Fig. 13), with low slope exponents resulting in high incision rates and few streams, and vice versa.

The effect of changes in hillslope diffusion rate on the development of streams is illustrated in Fig. 15. As many previous studies have highlighted (Tucker and Bras, 1998; Perron et al., 2008), hillslope diffusion competes with stream incision. High rates of diffusion result in high sediment fluxes toward streams. It is difficult for small streams to compete with these high rates of sediment delivery, and as a result only larger streams survive. In contrast, low rates of hillslope diffusion allow more streams to persist.

Interestingly, precipitation and specific yield have a limited effect on drainage density (Fig. 13). Precipitation affects groundwater recharge. Given that groundwater flow depends on the ratio of recharge over transmissivity (see eq. 13), in principle recharge has an effect of equal magnitude as transmissivity, but opposite sign. However, the variability of transmissivity of the subsurface is several orders of magnitude, whereas the variability of groundwater recharge is much lower, approximately one order of magnitude in humid regions (Moeck et al., 2020). This results in an overall much more important effect of transmissivity on drainage density.

Specific yield only has a subtle effect in that lower values of specific yield increase the volume of saturation overland flow and make it more difficult for streams to run completely dry, even if they are disconnected from the watertable. However, given the subordinate importance of overland flow in generating streamflow and erosion in these model experiments, this effect is very modest and does not change the modelled drainage density or incision rate after a model runtime of 100,000 years (Fig. 13).

Earth **Surface**
Dynamics
Discussions
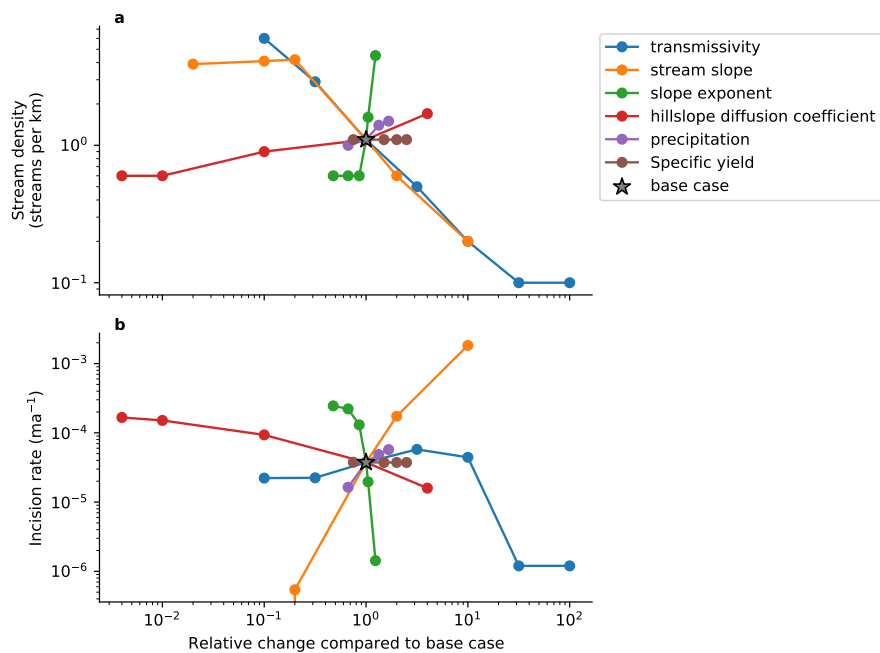
Figure 13. Sensitivity of drainage density and stream incision to hydrological and erosion parameters. The incision rate denotes the incision rate of the stream with the lowest elevation at the end of each model run. Note that the range of parameter values reflects their variability in humid and subhumid settings as explained in the text.
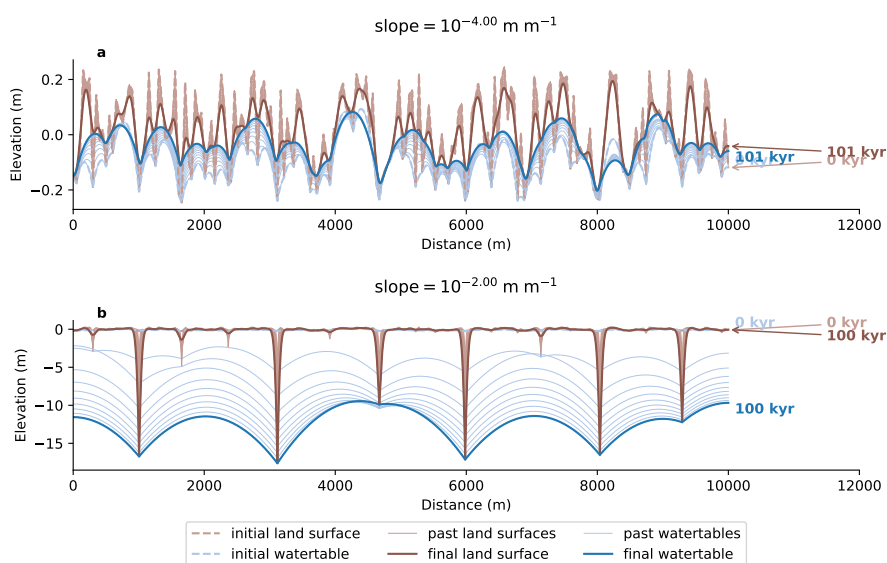
Figure 14. Sensitivity of drainage density and stream incision to initial slope, showing the effects of the lowest (panel a) and highest (panel b) slope that was included in the model sensitivity analysis. Low slopes result in a very low incision power, whereas high slopes provide much more incision power that allows the system to evolve to a situation with fewer active streams.
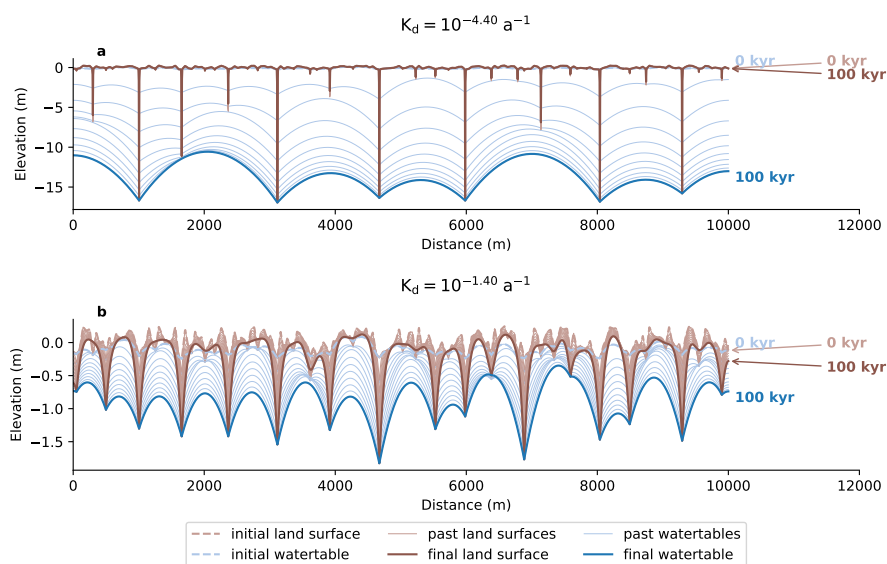
Figure 15. Sensitivity of drainage density and stream incision to hillslope diffusion rate, showing the effects of the lowest (panel a) and highest (panel b) hillslope diffusion rates found in a compilation by Richardson et al. (2019).

Earth **Surface**
Dynamics
Discussions

4 Discussion

370 ### 4.1 Limitations of the model code

The model code presented here was intentionally kept as simple as possible to keep the solution mathematically tractable and the computational effort manageable. The main limitations are that the model is 2.5D and only represents a system with perfectly parallel and straight streams, groundwater flow is steady-state and the contribution of transient groundwater discharge or subsurface stormflow to streamflow is neglected, and the treatment of erosion by overland flow is highly simplified, with

375 an instant addition of all overland flow to the nearest active stream channel, and a highly simplified distribution of the eroded volume over the length of the channel.

In spite of these limitations the conclusions of the importance of groundwater flow for drainage density and stream incision are arguably relatively robust. The model results show that groundwater capture is a somewhat inevitable consequence of coupling groundwater flow, streamflow and erosion equations. Regardless of the exact equations and numerical implementation

380 used, the watertable will always crop out at perennial streams, and the incision of these streams will draw the watertable down. Smaller streams losing their groundwater discharge and eventually falling dry is therefore a logical consequence of differences in incision rate between streams. These conclusions are also supported by previous model studies that found that groundwater flow had a strong effect on erosion (de Vries, 1994; Huang and Niemann, 2006; Barkwith et al., 2015; Zhang et al., 2016) and by observations that found a correlation between permeability, transmissivity, or lithology and drainage density at a number of

385 locations (Carlston, 1963; Luo and Stepinski, 2008; Bloomfield et al., 2011; Luo et al., 2016).

However, one thing that the model does not represent well is the initiation of stream channels. Due to the 2.5D nature of the model the initial topography is represented only in the modelled cross-section, and all streams are effectively parallel. This means that initially, small streams develop in most small depressions. The presence of many small streams divides the water to be discharged over many streams, which each have a very low incision power but are nonetheless considered active streams

390 in the model. In reality, many of these streams would not initiate, because the initial topography would not consist of a set of small depressions that are lined up and connected along an inclined slope. Instead, most of these depressions would be isolated. Therefore the number of active streams at low runtimes should be much smaller than the high number in the model runs reported here (see for example Fig. 11a). In reality, the stream network would develop much more gradually by headward erosion, as shown by natural experiments (Schumm, 1956; Wells et al., 1985; Kashiwaya, 1987; Talling and Sowter, 1999).

395 For the final model results presented in this study the unrealistic initiation of streams is less of a problem, because the stream networks adjusts relatively rapidly in the first few 100s to 1000s of years as stream incision progresses far enough for most of the initial streams to fall dry and for the initial topography to be irrelevant. Therefore for the final model runtime of a 100,000 years the unrealistic initiation of stream networks does not affect the results. The exception is however, formed by model runs with low transmissivity ($< 10^{-4}$ m^2 s^{-1}) or low intial slope ($< 10^{-4}$ m m^{-1}), for which the ability to capture groundwater

400 discharge and the incision power of the streams is too low to escape the initial phase with a dense stream network.

4.2 Groundwater capture

To my knowledge the process of groundwater capture that is illustrated here has not been proposed before. de Vries (1976) and de Vries (1994) discussed the opposite process, in which new streams establish themselves when the watertable reaches the land surface following an increase in precipitation and groundwater recharge. Twidale (2004) suggested that stream incision

405 may induce a positive feedback by increasing groundwater flow and runoff to streams that incise faster, but did not provide any further details.

The process of groundwater capture is expected to be important wherever streamflow is dominated either by groundwater discharge or saturation overland flow. In systems where infiltration-excess flow is dominant, which includes most semi-arid and arid regions (Kidron, 2021), groundwater capture could still occur and would determine which streams discharge groundwater

410 and are active perennially, but streams that are detached from the groundwater table would still be able to incise. In addition, groundwater capture may be less important for systems dominated by subsurface stormflow in perched aquifers that are detached from the watertable. The importance of this flow mechanism is however uncertain and under debate (Freeze, 1972; Chifflard et al., 2019).

Note that the difference between the groundwater capture process and the more well studied process of stream capture

415 (Whipple et al., 2017) is that groundwater capture does not require a physical connection between two streams, and may therefore not leave a clear trace in the landscape, as opposed to river capture. The capture of the groundwater discharge of one stream by another results in the first stream falling dry, but the hillslope between these streams remains intact, as can be seen in Fig. 10.

5 Conclusions

420 A new model is presented that couples equations that govern groundwater flow, overland flow, streamflow and erosion and represents humid regions where infiltration-excess overland flow is negligible. The coupling of these equations reveals a strong dependence of drainage density on groundwater flow and transmissivity. The dependence of drainage density on groundwater flow is controlled by a process identified here as groundwater capture, by which faster incising streams draw the watertable below neighbouring streams, which fall dry and lose the ability to incise any further. This process is more efficient when the

425 watertable is relatively flat, which can be either due to low groundwater recharge or high transmissivity, with transmissivity often being the dominant control due to its high variability. Sensitivity analysis show that the importance of transmissivity for drainage density is roughly equal to parameters that control the incision power of stream channels. The importance of transmissivity exceeds other hydrological and erosion parameters such as precipitation and hillslope diffusion coefficient. The results imply that groundwater and transmissivity may be a dominant control on drainage density in humid regions. Landscape

430 evolution models may need to include groundwater flow and the watertable. At the same time a closer integration of landscape and groundwater data and models may help improve knowledge of the evolution of the earth's surface.

Code availability. The model code presented in this manuscript is named the groundwater flow, overland flow and erosion model, GOEMod, and has been published at Zenodo (Luijendijk, 2021). The code is also available at GitHub (https://github.com/ElcoLuijendijk/goemod). The code is distributed under the GNU General Public License, version 3. The code includes a Jupyter notebook to execute a single model
435   run, which can be used to reproduce Fig. 9, 10 and 11 (https://github.com/ElcoLuijendijk/goemod/blob/master/goemod.ipynb), and a Python script to execute multiple model runs that can be used for model sensitivity analysis, such as presented in Fig. 13 (https://github.com/ElcoLuijendijk/goemod/blob/master/goemod_multiple_runs.py). GOEMod depends on the Python modules Numpy (Harris et al., 2020), Matplotlib (Hunter, 2007), Pandas (McKinney, 2010; Reback et al., 2021) and Scientific colour maps (Crameri, 2021).

Competing interests. The author declares that no competing interests are present

440   *Acknowledgements.* I would like to thank Co de Vries for sparking my interest in the relation between groundwater systems and landscape evolution.

References

Abrams, D. M., Lobkovsky, A. E., Petroff, A. P., Straub, K. M., McElroy, B., Mohrig, D. C., Kudrolli, A., and Rothman, D. H.: Growth laws for channel networks incised by groundwater flow, Nature Geoscience, 2, 193–196, https://doi.org/10.1038/ngeo432, 2009.

445 Barkwith, A., Hurst, M. D., Jackson, C. R., Wang, L., Ellis, M. A., and Coulthard, T. J.: Simulating the influences of groundwater on regional geomorphology using a distributed, dynamic, landscape evolution modelling platform, Environmental Modelling and Software, 74, 1–20, https://doi.org/10.1016/j.envsoft.2015.09.001, 2015.

Beersma, J., Hakvoort, H., Jilderda, R., Overeem, A., and Versteeg, R.: Neerslagstatistiek en -reeksen voor het waterbeheer 2019, Tech. rep., Stichting teogepast onderzoek waterbeheer, Amersfoort, 2019.

450 Bloomfield, J. P., Bricker, S. H., and Newell, A. J.: Some relationships between lithology, basin form and hydrology: A case study from the Thames basin, UK, Hydrological Processes, 25, 2518–2530, https://doi.org/10.1002/hyp.8024, 2011.

Bogaart, P. W., Tucker, G. E., and de Vries, J. J.: Channel network morphology and sediment dynamics under alternating periglacial and temperate regimes: A numerical simulation study, Geomorphology, 54, 257–277, https://doi.org/10.1016/S0169-555X(02)00360-4, 2003.

Bresciani, E., Goderniaux, P., and Batelaan, O.: Hydrogeological controls of water table-land surface interactions, Geophysical Research

455 Letters, 43, 9653–9661, https://doi.org/10.1002/2016GL070618, 2016.

Brocard, G., Teyssier, C., Dunlap, W. J., Authemayou, C., Simon-Labric, T., Cacao-Chiquín, E. N., Gutiérrez-Orrego, A., and Morán-Ical, S.: Reorganization of a deeply incised drainage: Role of deformation, sedimentation and groundwater flow, Basin Research, 23, 631–651, https://doi.org/10.1111/j.1365-2117.2011.00510.x, 2011.

Carlston, C. W.: Drainage density and streamflow, U.S. Geol. Surv. Prof. Pap. No. 42, pp. 2–C, 8pp, 1963.

460 Chifflard, P., Blume, T., Maerker, K., Hopp, L., van Meerveld, I., Graef, T., Gronz, O., Hartmann, A., Kohl, B., Martini, E., Reinhardt-Imjela, C., Reiss, M., Rinderer, M., and Achleitner, S.: How can we model subsurface stormflow at the catchment scale if we cannot measure it?, Hydrological Processes, 33, 1378–1385, https://doi.org/10.1002/hyp.13407, 2019.

Crameri, F.: Scientific colour maps, https://doi.org/10.5281/zenodo.4491293, https://doi.org/10.5281/zenodo.4491293, 2021.

Culling, W. E. H.: Analytical theory of erosion, The Journal of Geology, 68, 336–344, 1960.

465 Culling, W. E. H.: Soil Creep and the Development of Hillside Slopes, The Journal of Geology, 71, 127–161, https://doi.org/10.1086/626891, 1963.

de Vries, J. J.: The groundwater outcrop-erosion model; evolution of the stream network in The Netherlands, Journal of Hydrology, 29, 43–50, https://doi.org/10.1016/0022-1694(76)90004-4, 1976.

de Vries, J. J.: Dynamics of the interface between streams and groundwater systems in lowland areas, with reference to stream net evolution,

470 Journal of Hydrology, 155, 39–56, https://doi.org/10.1016/0022-1694(94)90157-0, 1994.

Dunne, T.: Field Studies of hillslope flow processes, in: Hillslope Hydrology, edited by Kirkby, M., chap. 7, pp. 227–293, John Wiley and sons, Chichester, 1978.

Dunne, T.: Hydrologyy mechanics, and geomorphic implications of erosion by subsurface flow, Special Paper of the Geological Society of America, 252, 1–28, https://doi.org/10.1130/SPE252-p1, 1990.

475 Dunne, T. and Black, R. D.: An Experimental Investigation of Runoff Production in Permeable Soils, Water Resources Research, 6, 478–490, https://doi.org/10.1029/WR006i002p00478, 1970.

El-husseiny, A.: Improved Packing Model for Functionally Graded Sand-Fines Mixtures — Incorporation of Fines Cohesive Packing Behavior, applied sciences, 10, 23–26, https://doi.org/10.3390/app10020562, 2020.

Forchheimer, P.: Über die Ergiebigkeit von Brunnen, Anlagen und Sickerschlitzen, Zeitsch Archit. Ing. Ver., Hannover, 32, 539–563, 1886.

480   Freeze, R. A.: Role of Subsurface Flow in Generating Surface Runoff 2. Upstream Source Areas, Water Resources Research, 8, 1272–1283, 1972.

Gauckler, P.: Etudes Théoriques et Pratiques sur l'Ecoulement et le Mouvement des Eaux, vol. 64, Gauthier-Villars, Paris, 1867.

Gleeson, T., Smith, L., Moosdorf, N., Hartmann, J., Dürr, H. H., Manning, A. H., van Beek, L. P. H., and Jellinek, A. M.: Mapping permeability over the surface of the Earth, Geophysical Research Letters, 38, 1–6, https://doi.org/10.1029/2010GL045565, 2011.

485   Gleeson, T., Moosdorf, N., Hartmann, J., and van Beek, L. P. H.: A glimpse beneath earth's surface: GLobal HYdrogeology MaPS (GL-HYMPS) of permeability and porosity, Geophysical Research Letters, 41, 1–8, https://doi.org/10.1002/2014GL059856, 2014.

Gleeson, T., Befus, K. M., Jasechko, S., Luijendijk, E., and Cardenas, M. B.: The global volume and distribution of modern groundwater, Nature Geoscience, 9, 161–167, https://doi.org/10.1038/ngeo2590, 2016.

Harel, M. A., Mudd, S. M., and Attal, M.: Global analysis of the stream power law parameters based on worldwide 10Be denudation rates, 490   Geomorphology, 268, 184–196, https://doi.org/10.1016/j.geomorph.2016.05.035, 2016.

Harris, C. R., Millman, K. J., van der Walt, S. J., Gommers, R., Virtanen, P., Cournapeau, D., Wieser, E., Taylor, J., Berg, S., Smith, N. J., Kern, R., Picus, M., Hoyer, S., van Kerkwijk, M. H., Brett, M., Haldane, A., del Río, J. F., Wiebe, M., Peterson, P., Gérard-Marchant, P., Sheppard, K., Reddy, T., Weckesser, W., Abbasi, H., Gohlke, C., and Oliphant, T. E.: Array programming with NumPy, Nature, 585, 357–362, https://doi.org/10.1038/s41586-020-2649-2, 2020.

495   Howard, A. D.: Badland morphology and evolution: Interpretation using a simulation model, Earth Surface Processes and Landforms, 22, 211–227, https://doi.org/10.1002/(SICI)1096-9837(199703)22:3<211::AID-ESP749>3.0.CO;2-E, 1997.

Huang, X. and Niemann, J. D.: Modelling the potential impacts of groundwater hydrology on long-term drainage basin evolution, Earth Surface Processes and Landforms, 31, 1802–1823, https://doi.org/https://doi.org/10.1002/esp.1369, https://onlinelibrary.wiley.com/doi/abs/10.1002/esp.1369, 2006.

500   Hunter, J. D.: Matplotlib: A 2D graphics environment, Computing in Science & Engineering, 9, 90–95, https://doi.org/10.1109/MCSE.2007.55, 2007.

Jasechko, S., Perrone, D., Befus, K. M., Bayani Cardenas, M., Ferguson, G., Gleeson, T., Luijendijk, E., McDonnell, J. J., Taylor, R. G., Wada, Y., and Kirchner, J. W.: Global aquifers dominated by fossil groundwaters but wells vulnerable to modern contamination, Nature Geoscience, 10, 425–429, https://doi.org/10.1038/ngeo2943, 2017.

505   Kashiwaya, K.: Theoretical investigation of the time variation of drainage density, Earth Surface Processes and Landforms, 12, 39–46, 1987.

Kidron, G. J.: Comparing overland flow processes between semiarid and humid regions: Does saturation overland flow take place in semiarid regions?, Journal of Hydrology, 593, 125 624, https://doi.org/10.1016/j.jhydrol.2020.125624, https://doi.org/10.1016/j.jhydrol.2020.125624, 2021.

Lacey, G.: Stable Channels in Alluvium, Minutes of the Proceedings of the Institution of Civil Engineers, 229, 259–292, 510   https://doi.org/10.1680/imotp.1930.15592, https://doi.org/10.1680/imotp.1930.15592, 1930.

Litwin, D. G., Tucker, G. E., Barnhart, K. R., and Harman, C. J.: GroundwaterDupuitPercolator: A Landlab component for groundwater flow, Journal of Open Source Software, 5, 1935, https://doi.org/10.21105/joss.01935, 2020.

Luijendijk, E.: GOEMod: groundwater flow, overland flow and erosion model, https://doi.org/10.5281/zenodo.4663728, 2021.

Luijendijk, E. and Gleeson, T.: How well can we predict permeability in sedimentary basins? Deriving and evaluating porosity-permeability 515   equations for noncemented sand and clay mixtures, Geofluids, 15, 67–83, https://doi.org/10.1111/gfl.12115, https://doi.org/10.1111/gfl.12115, 2015.

Luo, W. and Pederson, D. T.: Hydraulic conductivity of the High Plains Aquifer re-evaluated using surface drainage patterns, Geophysical Research Letters, 39, 1–6, https://doi.org/10.1029/2011GL050200, 2012.

Luo, W. and Stepinski, T.: Identification of geologic contrasts from landscape dissection pattern: An application to the Cascade Range, Oregon, USA, Geomorphology, 99, 90–98, https://doi.org/10.1016/j.geomorph.2007.10.014, 2008.

Luo, W., Grudzinski, B. P., and Pederson, D.: Estimating hydraulic conductivity from drainage patterns-a case study in the Oregon Cascades, Geology, 38, 335–338, https://doi.org/10.1130/G30816.1, 2010.

Luo, W., Jasiewicz, J., Stepinski, T., Wang, J., Xu, C., and Cang, X.: Spatial association between dissection density and environmental factors over the entire conterminous United States, Geophysical Research Letters, 43, 692–700, https://doi.org/10.1002/2015GL066941, 2016.

Manning, R.: On the flow of water in open channels and pipes, Transactions of the Institution of Civil Engineers of Ireland, 20, 161–207, 1891.

McKinney, W.: Data Structures for Statistical Computing in Python, in: Proceedings of the 9th Python in Science Conference, edited by van der Walt, S. and Millman, J., pp. 56–61, https://doi.org/10.25080/Majora-92bf1922-00a, 2010.

Moeck, C., Grech-Cumbo, N., Podgorski, J., Bretzler, A., Gurdak, J. J., Berg, M., and Schirmer, M.: A global-scale dataset of direct natural groundwater recharge rates: A review of variables, processes and relationships, Science of The Total Environment, 717, 137 042, https://doi.org/https://doi.org/10.1016/j.scitotenv.2020.137042, 2020.

Montgomery, D. R. and Dietrich, W. E.: Channel Initiation and the Problem of Landscape Scale, Science, 255, 826 LP – 830, https://doi.org/10.1126/science.255.5046.826, 1992.

Pederson, D. T.: Stream piracy revisited: A groundwater-sapping solution, GSA Today, 11, 4–11, 2001.

Perron, J. T., Dietrich, W. E., and Kirchner, J. W.: Controls on the spacing of first-order valleys, Journal of Geophysical Research: Earth Surface, 113, https://doi.org/10.1029/2007JF000977, 2008.

Perron, J. T., Kirchner, J. W., and Dietrich, W. E.: Formation of evenly spaced ridges and valleys, Nature, 460, 502–505, https://doi.org/10.1038/nature08174, 2009.

Perron, J. T., Richardson, P. W., Ferrier, K. L., and Lapotre, M.: The root of branching river networks, Nature, 492, 100–103, https://doi.org/10.1038/nature11672, 2012.

Reback, J., McKinney, W., Jbrockmendel, den Bossche, J. V., Augspurger, T., Cloud, P., Gfyoung, Hawkins, S., Sinhrks, Roeschke, M., Klein, A., Petersen, T., Tratner, J., She, C., Ayd, W., Naveh, S., Garcia, M., Schendel, J., Patrick, Hayden, A., Saxton, D., Jancauskas, V., McMaster, A., Gorelli, M., Battiston, P., Seabold, S., Dong, K., Chris-b1, H-vetinari, and Hoyer, S.: pandas-dev/pandas: Pandas 1.2.2, https://doi.org/10.5281/zenodo.4524629, 2021.

Revil, A.: Mechanical compaction of sand/clay mixtures, Journal of Geophysical Research, 107, https://doi.org/10.1029/2001JB000318, http://www.agu.org/pubs/crossref/2002/2001JB000318.shtml, 2002.

Richardson, P. W., Perron, J. T., and Schurr, N. D.: Influences of climate and life on hillslope sediment transport, Geology, 47, 423–426, https://doi.org/10.1130/G45305.1, 2019.

Schumm, S. A.: Evolution of draiange systems and slopes in badlands at Perth Amboy, New Jersey, Bulletin of the Geological Society of America, 67, 579–646, 1956.

Talling, P. J. and Sowter, M. J.: Drainage density on progressively tilted surfaces with different gradients, Wheeler Ridge, California, Earth Surface Processes and Landforms, 24, 809–824, https://doi.org/10.1002/(SICI)1096-9837(199908)24:9<809::AID-ESP13>3.0.CO;2-R, 1999.

Tucker, G., Lancaster, S., Gasparini, N., and Bras, R.: The channel-hillslope integrated landscape development model (CHILD), in: Landscape erosion and evolution modeling, pp. 349–388, Springer, 2001a.

Tucker, G. E. and Bras, R. L.: Hillslope processes, drainage density and landscape morphology, Water Resources Research, 34, 2751–2764, https://doi.org/doi:10.1029/98WR01474, http://dx.doi.org/10.1029/98WR01474, 1998.

Tucker, G. E. and Hancock, G.: Modelling landscape evolution, Earth Surface Processes and Landforms, 35, 28–50, https://doi.org/10.1002/esp, http://doi.wiley.com/10.1002/esp.1730, 2010.

Tucker, G. E., Catani, F., Rinaldo, A., and Bras, R. L.: Statistical analysis of drainage density from digital terrain data, Geomorphology, 36, 187–202, https://doi.org/10.1016/S0169-555X(00)00056-8, 2001b.

Twidale, C. R.: River patterns and their meaning, Earth-Science Reviews, 67, 159–218, https://doi.org/10.1016/j.earscirev.2004.03.001, 2004.

van den Berg, J. H.: Prediction of alluvial channel pattern of perennial rivers, Geomorphology, 12, 259–279, https://doi.org/10.1016/0169-555X(95)00014-V, 1995.

van der Meij, W. M., Temme, A., Lin, H. S., Gerke, H. H., and Sommer, M.: On the role of hydrologic processes in soil and landscape evolution modeling: concepts, complications and partial solutions, Earth-Science Reviews, 185, 1088–1106, https://doi.org/10.1016/j.earscirev.2018.09.001, 2018.

Wells, S. G., Dohrenwend, J. C., McFadden, L. D., Turrin, B. D., and Mahrer, K. D.: Late Cenozoic landscape evolution on lava flow surfaces of the Cima volcanic field, Mojave Desert, California., Geological Society of America Bulletin, 96, 1518–1529, https://doi.org/10.1130/0016-7606(1985)96<1518:LCLEOL>2.0.CO;2, 1985.

Whipple, K. X., Forte, A. M., DiBiase, R. A., Gasparini, N. M., and Ouimet, W. B.: Timescales of landscape response to divide migration and drainage capture: Implications for the role of divide mobility in landscape evolution, Journal of Geophysical Research: Earth Surface, 122, 248–273, https://doi.org/10.1002/2016JF003973, 2017.

Zhang, Y., Slingerland, R., and Duffy, C.: Fully-coupled hydrologic processes for modeling landscape evolution, Environmental Modelling and Software, 82, 89–107, https://doi.org/10.1016/j.envsoft.2016.04.014, 2016.